nature materials

LETTERS

PUBLISHED ONLINE: 1 JULY 2012 | DOI: 10.1038/NMAT3357

Rapid casting of patterned vascular networks for perfusable engineered three-dimensional tissues

Jordan S. Miller[1], Kelly R. Stevens[2], Michael T. Yang[1], Brendon M. Baker[1], Duc-Huy T. Nguyen[1], Daniel M. Cohen[1], Esteban Toro[1], Alice A. Chen[2], Peter A. Galie[1], Xiang Yu[1], Ritika Chaturvedi[1], Sangeeta N. Bhatia[2,3,4] and Christopher S. Chen[1]*

In the absence of perfusable vascular networks, three-dimensional (3D) engineered tissues densely populated with cells quickly develop a necrotic core[1]. Yet the lack of a general approach to rapidly construct such networks remains a major challenge for 3D tissue culture[2–4]. Here, we printed rigid 3D filament networks of carbohydrate glass, and used them as a cytocompatible sacrificial template in engineered tissues containing living cells to generate cylindrical networks that could be lined with endothelial cells and perfused with blood under high-pressure pulsatile flow. Because this simple vascular casting approach allows independent control of network geometry, endothelialization and extravascular tissue, it is compatible with a wide variety of cell types, synthetic and natural extracellular matrices, and crosslinking strategies. We also demonstrated that the perfused vascular channels sustained the metabolic function of primary rat hepatocytes in engineered tissue constructs that otherwise exhibited suppressed function in their core.

Living tissues have complex mass transport requirements that are principally met by blood flow through multiscale vascular networks of the cardiovascular system. Such vessels deliver nutrients and oxygen to, and remove metabolic byproducts from, all of the organ systems in the body and were critical to the rise of large-scale multicellular organisms[5]. Although tremendous progress has been made in the past few decades to isolate and culture cells from native tissues, simple methods to generate tissue constructs populated at physiologic cell densities that are sustained by even the most basic vascular architectures have remained elusive.

To create perfusable channels in engineered tissues, layer-by-layer assembly[6–9] has been explored. In this approach, a trench is moulded into one layer such that a second, separately fabricated layer can then be aligned and laminated to close the lid to form channels in an iterative fashion. However, layer-by-layer assembly is slow and results in seams or other structural artefacts throughout the construct while simultaneously placing considerable design constraints on the materials, channels, and cells used during fabrication. Bioprinting[10], in which cells and matrix are deposited dropwise, has been developed over the past decade but also is a slow, serial process with limitations on print resolution, materials, and cells. In contrast to these methods, 3D sacrificial moulding[11–13] provides an intriguing alternative. Proof-of-concept studies have shown that a network of channels can be fabricated by creating a rigid 3D lattice of filaments, casting the lattice into a rubber or plastic material, and then sacrificing the lattice to reveal a microfluidic architecture in the bulk material. However, 3D sacrificial moulding of perfusable channels has so far required the use of cytotoxic organic solvents or processing conditions for either removing the sacrificial filaments or casting the surrounding material, and thus could not be accomplished with aqueous-based extracellular matrices (ECMs) or in the presence of living cells.

Here, we describe a biocompatible sacrificial material—a simple glass made from mixtures of inexpensive and readily available carbohydrates—and a means to print the material to facilitate the rapid casting of patterned 3D vascular networks in engineered tissues. This carbohydrate glass formulation was developed specifically to accommodate two seemingly opposing design criteria that we identified for biocompatible 3D sacrificial materials: sufficient mechanical stiffness to physically support its own weight in an open 3D lattice of filaments and the ability to dissolve rapidly and biocompatibly in the presence of living cells.

Carbohydrate glass can be formed by dissolving one or more carbohydrates in water and then boiling off the solvent. Our early experiments were based on a sucrose–glucose mixture developed by the food industry, which showed that although sucrose is unstable in supersaturated solutions, the addition of glucose prevents recrystallization and facilitates the formation of a stable and inexpensive glass[14]. This simple mixture was too hygroscopic and soft to handle. During material optimization and screening of potential additives, we found that the addition of starch stiffened the base material, but it imparted inferior optical clarity and therefore limited potential use with matrices that are commonly crosslinked by photochemical reactions[15,16]. In contrast, the addition of glycerol preserved clarity but rendered filaments mechanically unstable at room temperature. Ultimately, we further reinforced the glass and improved its temperature stability by incorporating dextrans. Uniaxial compression testing confirmed that the carbohydrate glass is mechanically stiff and brittle at room temperature (Fig. 1a). The optical transparency of the glass indicated compatibility with photopolymerization wavelengths in the ultraviolet, visible, and near-infrared ranges, making it unlikely that the glass would leave shadowing artefacts in photoactive scaffolds (Fig. 1b).

Multiscale vascular networks comprise a range of diameters of vessels and their interconnections. Thermal extrusion and fibre drawing with a 3D printer—a programmable Cartesian coordinate positioning system—provided an effective route to the fabrication of filamentous carbohydrate glass lattices. By

[1]Department of Bioengineering, University of Pennsylvania, Philadelphia, Pennsylvania 19104, USA, [2]Harvard-MIT Division of Health Sciences and Technology, Massachusetts Institute of Technology, Cambridge, Massachusetts 02139, USA, [3]Howard Hughes Medical Institute, Cambridge, Massachusetts 02139, USA, [4]Department of Electrical Engineering and Computer Science, Massachusetts Institute of Technology, Cambridge, Massachusetts 02139, USA. *e-mail: chrischen@seas.upenn.edu.

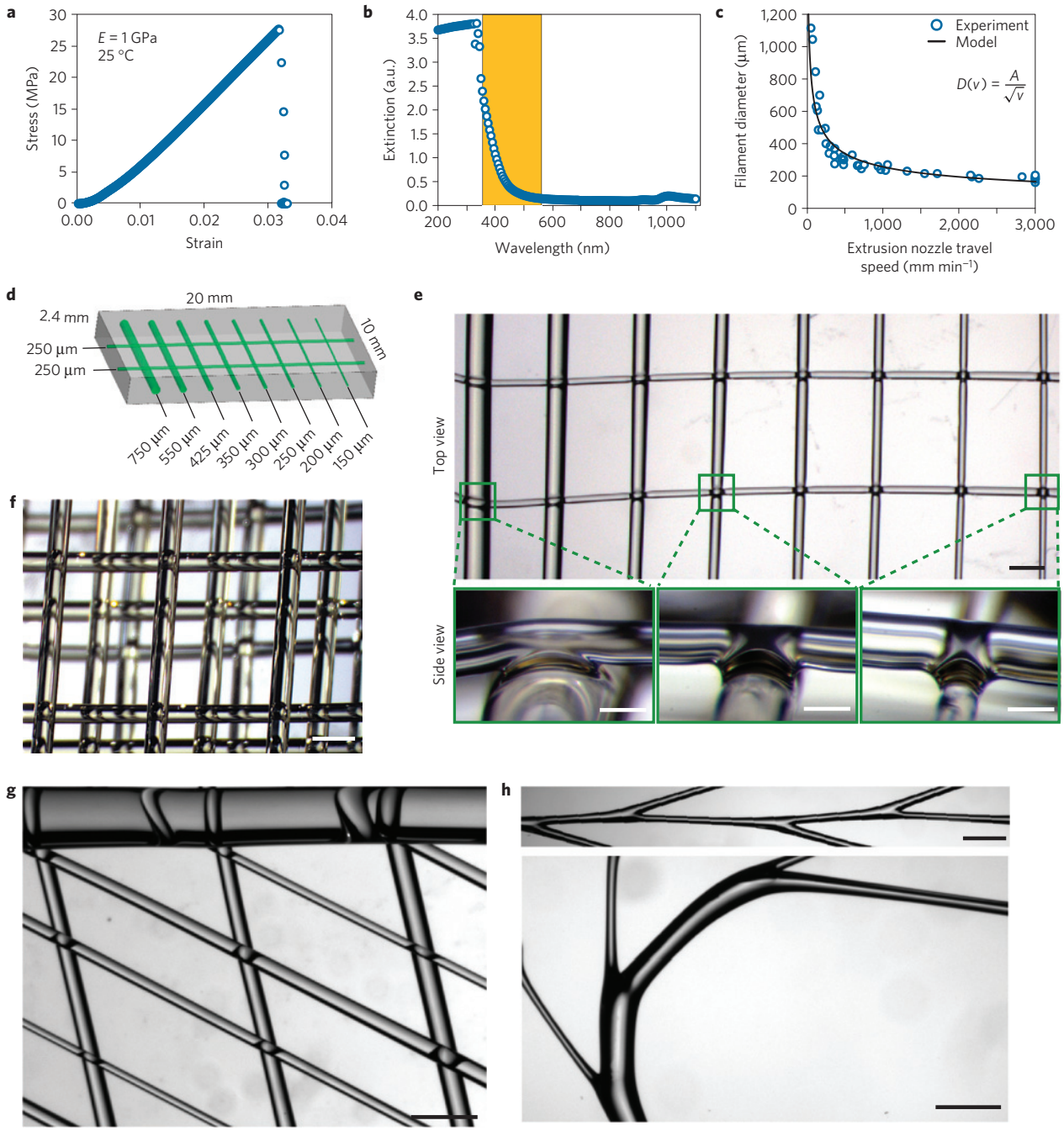

Figure 1 | Carbohydrate-glass material properties and filament-architecture formation. a, Stress–strain curve from uniaxial compression testing indicates that the carbohydrate glass is a stiff and brittle material at 25 °C, with Young's modulus $E = 1$ GPa (measured in the linear regime), maximum strength of 28 MPa and maximum strain of 3.25%. **b**, Optical extinction for a 1 cm sample of carbohydrate glass indicates that the material transmits light wavelengths commonly used during biocompatible imaging and photopolymerization (365–550 nm, shaded box). **c**, During thermal extrusion and 3D printing, filament diameter is controlled by the travel speed of the extrusion nozzle and follows a simple power law from glass-fibre drawing (equation inset). **d**, Architectural design of a multiscale carbohydrate-glass lattice (green). **e**, Top view of the multiscale architectural design in **d** printed in carbohydrate glass (scale bar, 1 mm). Interfilament melt fusions are magnified and shown in side-view (scale bars, 200 μm). **f**, Multilayered lattices are fabricated in minutes with precise lateral and axial positioning resolution (scale bar, 1 mm). **g**, A multiscale architecture showing a single 1 mm filament (top) connected to angled arrays of smaller interconnected filaments (scale bar, 1 mm). **h**, Serial *y*-junctions and curved filaments can also be fabricated (scale bars, 1 mm).

varying only the translational velocity of the extrusion nozzle, while holding constant the nozzle diameter and the extrusion flow rate parameters, extruded filament diameters tracked the governing equation:

$$D(v) = \frac{A}{\sqrt{v}}$$

where $D(v)$ is the resultant filament diameter, A is a constant that incorporates the extrusion nozzle diameter and extrusion flow rate, and v is the velocity of the extrusion nozzle (Fig. 1c). This relationship derives from existing models of glass-fibre drawing[17] and allowed the generation of carbohydrate-glass lattices in predefined, multiscale, and reproducible patterns (Fig. 1d–h). Moreover, controlling the temperature of the assembly platform

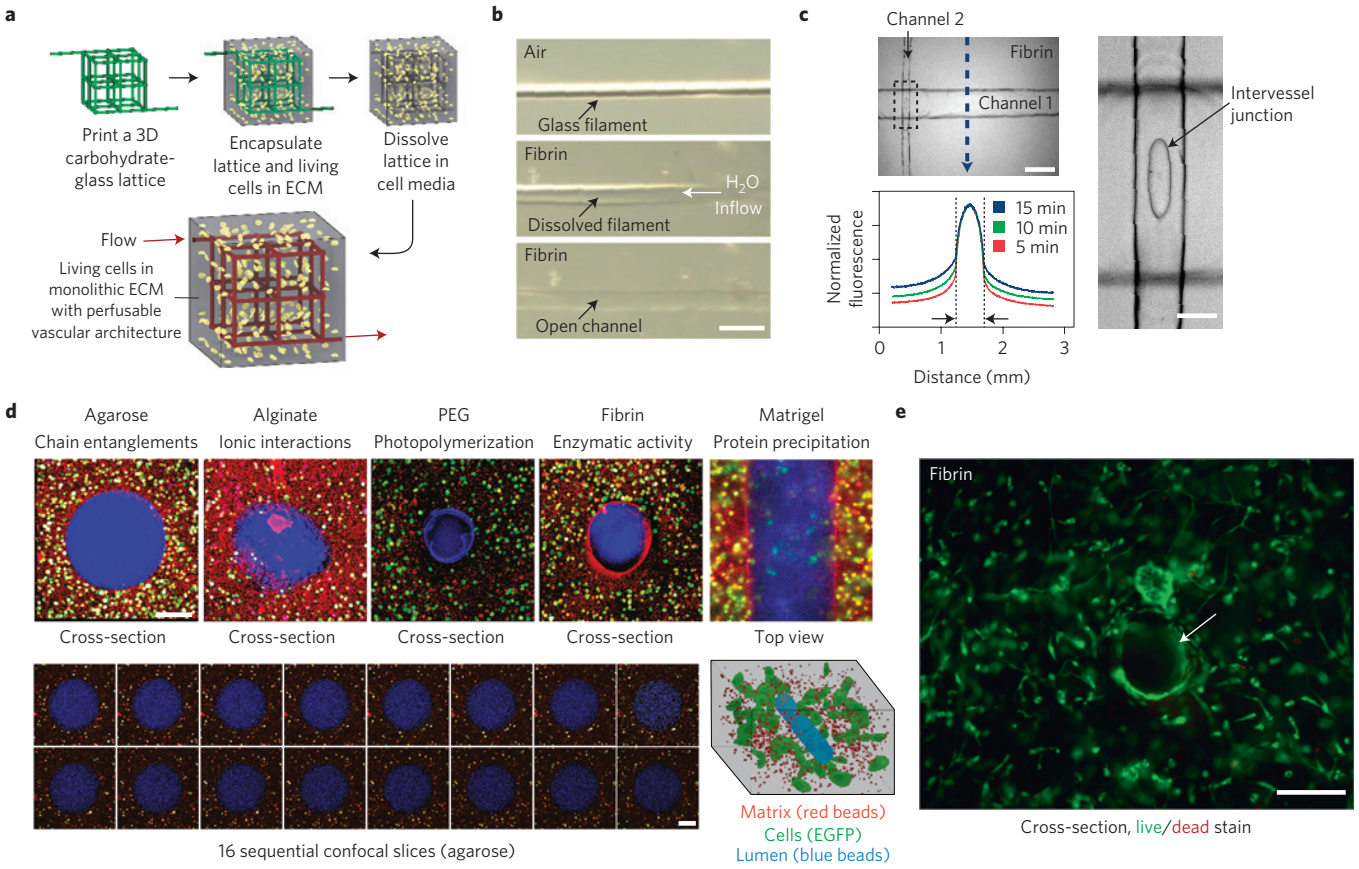

Figure 2 | Monolithic tissue construct containing patterned vascular architectures and living cells. a, Schematic overview. An open, interconnected, self-supporting carbohydrate-glass lattice is printed to serve as the sacrificial element for the casting of 3D vascular architectures. The lattice is encapsulated in ECM along with living cells. The lattice is dissolved in minutes in cell media without damage to nearby cells. The process yields a monolithic tissue construct with a vascular architecture that matches the original lattice. **b**, A single carbohydrate-glass fibre (200 μm in diameter, top) is encapsulated in a fibrin gel. Following ECM crosslinking, the gel and filament are immersed in aqueous solution and the dissolved carbohydrates are flowed out of the resulting channel (middle). Removal of the filament yields an open perfusable channel in the fibrin gel (bottom, scale bar, 500 μm). See Supplementary Movie S1 for full-time course. **c**, A fibrin gel with patterned interconnected channels of different diameters supports convective and diffusive transport of a fluorescent dextran injected into the channel network (upper left, phase contrast, scale bar, 500 μm). Line plot of normalized fluorescence across the gel and channel (blue arrow) shows a sinusoidal profile in the channel (between dotted black lines) characteristic of a cylinder and temporal diffusion from the channel into the bulk gel. Enlargement of the dotted box region shows an oval intervessel junction between the two perpendicular channels (right, scale bar, 100 μm). **d**, Cells constitutively expressing enhanced green fluorescent protein (EGFP) were encapsulated (5×10^6 ml^{-1}) in a variety of ECM materials and then imaged with confocal microscopy to visualize the matrix (red beads), cells (10T1/2, green) and the perfusable vascular lumen (blue beads). They are also shown schematically (bottom right). The materials have varied crosslinking mechanisms (annotated above the images) but were all able to be patterned with vascular channels. Scale bars, 200 μm. **e**, Representative cross-section image of unlabelled HUVEC (1×10^6 ml^{-1}) and 10T1/2 (1×10^6 ml^{-1}) co-cultures (not expressing EGFP) encapsulated uniformly in the interstitial space of a fibrin gel (10 mg ml^{-1}) with perfusable networks after two days in culture were stained with a fluorescent live/dead assay (green, Calcein AM; red, Ethidium Homodimer). Cells survive and spread near open cylindrical channels (highlighted with white arrow). Scale bar, 200 μm.

facilitated the formation of smooth melt fusions at filament intersections (Fig. 1e).

We next sought to use these lattices as a sacrificial element for creating fluidic channels within monolithic cellularized tissue constructs (Fig. 2a). In our strategy, a suspension of cells in ECM prepolymer is poured to encapsulate the lattice. After crosslinking the ECM, the glass filaments are dissolved to form vessels while their interfilament fusions become intervessel junctions (Fig. 2b,c). To prevent disruption of ECM crosslinking and to avoid the potential for osmotic damage to encapsulated cells due to carbohydrate dissolution, we coated the carbohydrate-glass lattice with a thin layer of poly(D-lactide-co-glycolide) (PDLGA) before casting the ECM. This coating allowed the dissolved carbohydrates to be flowed out of the formed channels instead of through the bulk of the engineered construct (Fig. 2b and Supplementary Movie S1). Importantly, the coating did not inhibit the ability of the network to support convective and diffusive transport into the bulk gel (Fig. 2c). Furthermore, we observed that, after sacrifice, the glass interfilament fusions left behind smooth elliptical intervessel junctions that supported fluidic connection between adjoining vascular channels.

To demonstrate the flexibility and generality of this approach, we patterned vascular channels in the presence of living cells in a wide range of natural and synthetic ECM materials (Fig. 2d). The time required for encapsulating cells and lattices in ECM prepolymer, ECM crosslinking, and glass dissolution is on the order of minutes. Importantly, we chose ECM materials which varied not only in their bulk material properties but also in their means of crosslinking. Indeed, the approach generated channels without the need to modify handling of aqueous cellularized gels formed by chain entanglements (cooling of agarose), ionic interactions (calcium-polymerized alginate), photopolymerization (synthetic

poly(ethylene glycol) (PEG)-based hydrogels[18]), enzymatic activity (thrombin-polymerized fibrin), and protein precipitation (warming of Matrigel). As predicted from the characterization of the optical transparency of the carbohydrate glass (Fig. 1b), photopolymerized gels exhibited no visible shadowing artefacts due to light absorption by the patterned glass lattice. To our knowledge, no other channel-forming technique is compatible with such a wide range of ECM materials. The approach also seems to have no negative effects on cells. Encapsulated cells survived, spread, and migrated in channelled scaffolds at levels not different from non-channelled control gels, demonstrating biocompatibility of the entire vessel casting process (Fig. 2e). Similar viability was found for human umbilical vein endothelial cells (HUVECs), 10T1/2 cells, human fibroblasts, and human embryonic kidney (HEK) cells (data not shown).

Owing to the mechanical rigidity and self-supporting nature of the carbohydrate-glass lattice, introducing a 3D multilayer architecture into the engineered vasculature requires no additional constraints, time, or steps to the sacrificial process (Supplementary Fig. S1a). To demonstrate the compatibility of this vascular casting approach with additional design considerations often important to the engineering of tissues, we fabricated complex cellular and immobilized-factor gradients in tissue constructs that also contained our channels (Supplementary Fig. S1b). Analysis of these tissue constructs (Supplementary Fig. S1c) demonstrated that patterning of cells or immobilized factors within the construct into step, linear, and exponential gradients could be accomplished in a single engineered tissue construct containing perfusable vascular channels. Here, cells were encapsulated along with immobilized fluorescent beads as a model factor, but this technology should be readily translated to immobilized gradients of adhesive peptides[19], proteins and growth factors[20–22], or the ECM itself[23,24]. Together, these results illustrate that the available design parameter space for a tissue construct is, for the first time, unhindered by the inclusion of patterned vascular channels and junctions.

Vascularized solid tissues can be conceptually reduced to a 'vascular unit cell' consisting of three key compartments: the vascular lumen, which serves as both the source and sink for most soluble factors; endothelial cells lining the vascular wall, which regulate mass-transport exchange with the interstitium; and cells and matrix residing in the interstitial zone between vascular channels (Fig. 3a). Here, we demonstrate control over each of these compartments in engineered tissue constructs. The monolithic nature of the gels (resulting from a single step polymerization) and the lack of architectural seams supported non-leaking perfusion of human blood under positive pressure with either laminar or turbulent pulsatile flow (Fig. 3b and Supplementary Movies S2 and S3), with smooth interchannel junctions supporting branched fluid flow. Endothelial cells seeded through a single inlet in the network quickly lined the walls of the entire network, including the junctions between vessels of differing diameters (Fig. 3c,d). Because this endothelium is formed after forming the tissue, these cells and their seeding are independently introduced from cells encapsulated in the interstitial zone. In co-cultures with 10T1/2 cells in the interstitial space, endothelial cells lining the vascular lumen became surrounded by the 10T1/2 cells and formed single and multicellular sprouts extending from the patterned vasculature into the bulk gel (Fig. 3e,f).

Engineered constructs densely populated with cells can develop a necrotic core owing to lack of adequate mass transport[1]. Thus, a major functional requirement of such an engineered vasculature is its utility to sustain cellular activity in metabolically demanding settings such as physiologically high cell densities. To facilitate imaging of such a densely populated construct, we generated a single layer of parallel fluidic channels formed within the centre of a rectangular construct. As a measure of cellular function and activity, we examined expression of destabilized enhanced green fluorescent protein (dsEGFP) from a constitutively expressed lentiviral cassette inserted into HEK293T cells. Monolithic slab gels uniformly distributed with cells exhibited cellular activity only at the gel perimeter (Fig. 4a). In contrast, gels with channels rescued protein expression in the gel core, most dramatically around each perfused channel. This preservation of cell function was perfusion-dependent, as dsEGFP expression was absent near channels without perfusion (data not shown). We also looked at a broader range of cellular densities in these constructs with a functional enzyme assay of a constitutively secreted Gaussia luciferase reporter. At low cell densities, diffusion alone is able to maintain cellular function in bulk gels (Fig. 4b). As nutrient requirements of the tissue construct increased with cell density, Gaussia production began to plateau. This limitation was overcome by convective transport through the channelled scaffold. The maintenance of cellular metabolic activity (Fig. 4a) as well as secretion of functional proteins and enzymes (Fig. 4b) are important functional outputs for many types of engineered tissues[25], both of which seem to be maintained with our engineered vasculature. Together these results illustrate the capacity of patterned perfusable channel architectures to provide functional mass transport to 3D cell cultures at or near physiologic cell densities.

Although these data demonstrate the utility of the approach in supporting a transformed cell line, primary parenchymal cells that would ultimately be required for clinically implanted engineered tissues often cannot tolerate stresses associated with extended periods of suspension and hypoxia. We therefore engineered perfusable gels containing primary hepatocytes, which are known to be highly sensitive to hypoxia and handling (Fig. 4c,d). After eight days in culture, perfusable tissues exhibited substantially higher albumin secretion and urea synthesis than slab gels (gels without channels) of the same volume (Fig. 4d). Optical sections of these constructs showed that at high cell concentrations cell survival was most prevalent adjacent to perfused channels and decayed radially, consistent with patterns observed in the dsEGFP-expressing HEK293T cells as well as with a 3D finite-element model of nutrient delivery to the entrapped cells (Supplementary Fig. S2). Together these results illustrate the utility of this strategy for supporting the function of engineered tissues comprising even highly sensitive primary cells.

Existing methods to create cell-laden gels containing a microfluidic network have required the delicate process of precise stacking and lamination of individually fabricated layers[6–9]. In this study, we found sacrificial carbohydrate-glass lattices to be well suited for the creation of densely populated tissue constructs with perfusable vascular channels and junctions. A key advantage of our method is that the entire perfusable scaffold is formed as a continuous phase simply by filling the 3D void volume around carbohydrate-glass lattices and by crosslinking the matrix. Cells are encapsulated in ECM and the resulting tissue construct can be perfused within minutes. We believe the sheer rapidity of this process prevents the formation of a necrotic core for metabolically demanding cells during fabrication. Moreover, the microstructural characteristics of the fluidic network—such as vessel diameter, circularity, surface roughness, and junction architecture—arise from fibre drawing and surface tension rather than photolithography or micromachining. Relying on simple physical principles, rather than on engineering processes, enabled the use of low-precision hardware to rapidly and reproducibly generate multiscale microvascular architectures in aqueous-based biomaterial scaffolds containing living cells.

Further, the process separation between the 3D microfabrication of filament networks and the handling of cells and ECM allows the dissemination of the technology to distant research laboratories. To illustrate this feature in the current study, carbohydrate-glass lattices were shipped under ambient conditions between laboratories. Primary liver hepatocytes were then encapsulated via standard manual pipetting steps to rapidly create perfusable hepatic

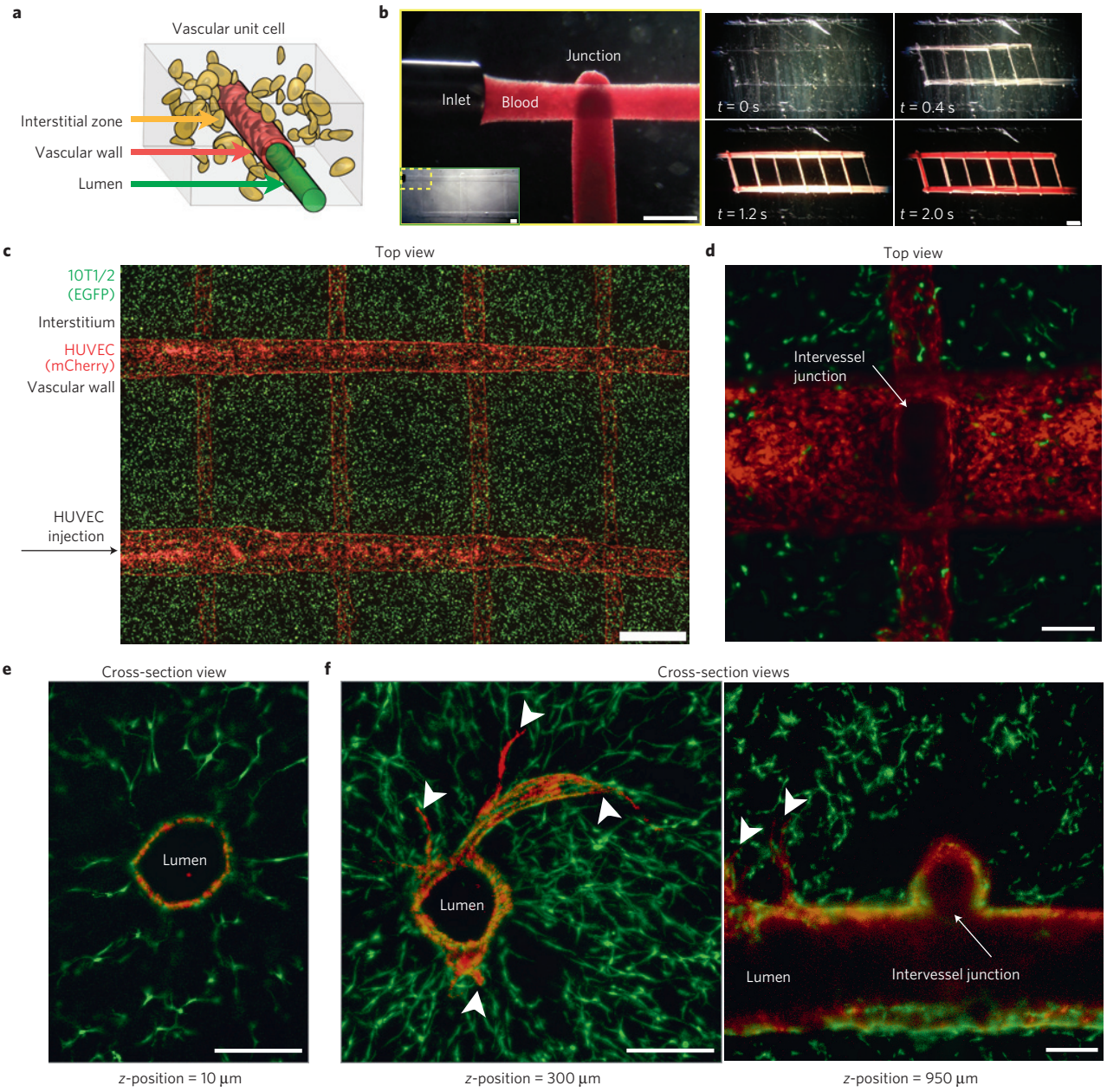

Figure 3 | Demonstrated control over the three key compartments of vascularized solid tissues. a, Schematic of these three compartments in a 'vascular unit cell' consisting of the vascular lumen, endothelial cells lining the vascular wall, and the interstitial zone containing matrix and encapsulated cells. **b**, Patterned vascular channels support positive pressure and pulsatile flow of human blood with intervessel junctions supporting branched fluid flow (left). Spiral flow patterns (right, 0.4 s) are characteristic of non-laminar flow through cylindrical channels. See Supplementary Movies S2 and S3; Scale bars, 1 mm, left; 2 mm, right. **c**, Control of the interstitial zone and the lining endothelium of vascularized tissue constructs is demonstrated by encapsulating 10T1/2 cells (1.5×10^6 ml^{-1}, constitutively expressing EGFP) in the interstitial space of a fibrin gel (10 mg ml^{-1}) followed by seeding of HUVECs (constitutively expressing mCherry) throughout the vascular network via a single lumenal injection (see Methods). After one day in culture a confocal *z*-stack montage demonstrated HUVECs residing in the vascular space with 10T1/2 uniformly distributed throughout the bulk gel. Scale bar, 1 mm. **d**, A partial *z*-stack of two intersecting channels demonstrated endothelialization of channel walls and across the intervessel junction, while in the surrounding bulk gel 10T1/2 cells are seen beginning to spread out in three dimensions. See Supplementary Movie S4 for the complete 700 μm *z*-stack from **d**. **e**, After nine days in culture, cross-section imaging of a representative channel (optical thickness and *z*-position = 10 μm) demonstrated that the endothelial monolayer lining the vascular lumen became surrounded by 10T1/2 cells. Scale bar, 200 μm. **f**, Endothelial cells formed single and multicellular sprouts (arrowheads) from patterned vasculature, as seen in a *z*-stack (optical thickness = 200 μm) from deeper within the gel (*z*-position = 300 μm, left). Even deeper imaging (*z*-position = 950 μm, optical thickness = 100 μm, right) confirmed that the vascular lumen remained open throughout vessels and intervessel junctions and that endothelial cells also sprouted from larger vessels (arrowheads). See Supplementary Movie S5 for the complete 1 mm *z*-stack from **e**,**f**.

tissues or non-perfusable control gels. The ability to access this vascularization strategy without fabricating the networks in-house may facilitate rapid adoption of the technology.

Engineered 3D constructs have gained increased attention as *in vitro* tools for the study of cell–cell and cell–matrix interactions, and are being explored for potential use as experimental models

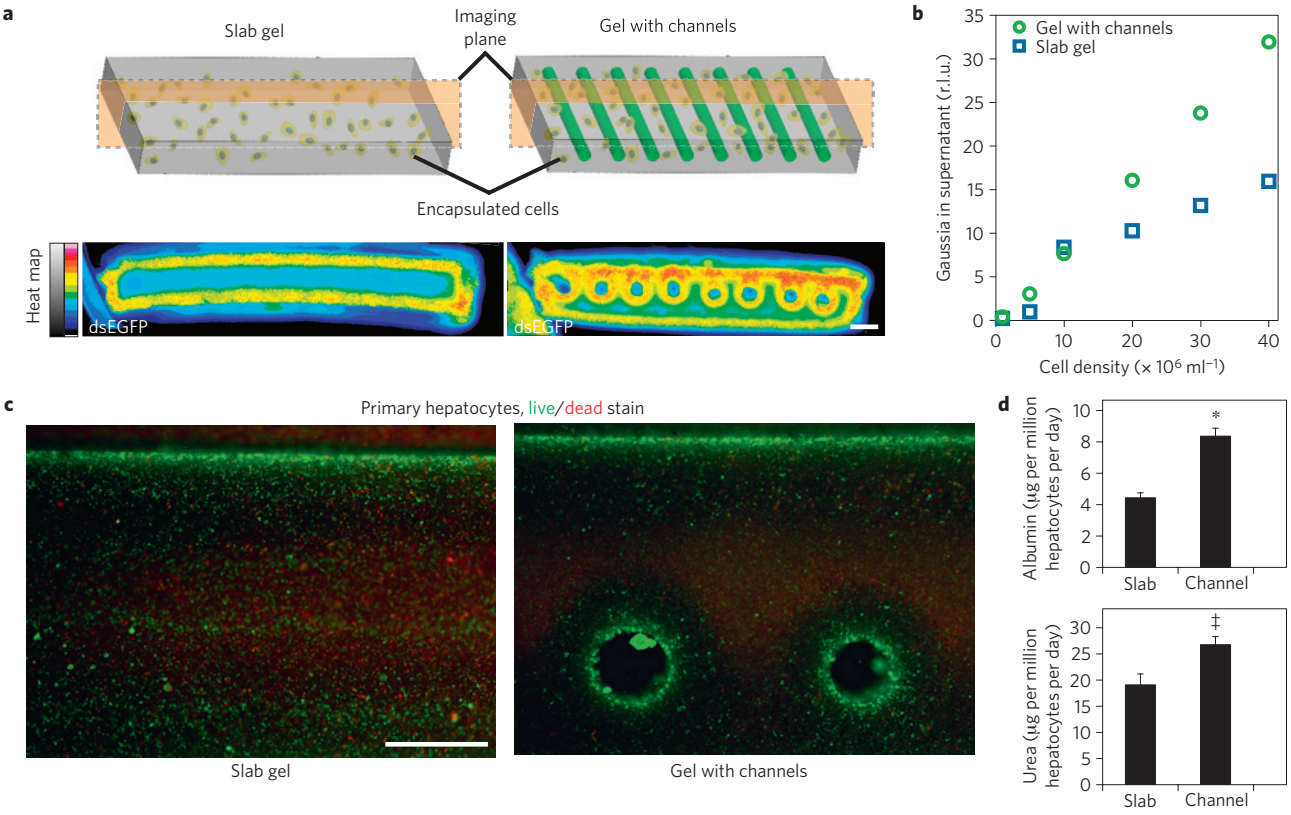

Figure 4 | Perfusion of channels sustains cellular metabolic function in the core of thick, densely populated tissue constructs. a, Representative cross-section image montages of PEG hydrogels containing 40×10^6 HEK cells ml^{-1} after three days in culture. The intracellular dsEGFP reporter spatially indicates that cells are active at the gel slab perimeter and circumferentially around perfusion channels, but not elsewhere in the gel core. Scale bar, 2 mm. **b**, A functional enzyme assay of secreted Gaussia luciferase from these constructs indicates that the channel architecture preserves cell function even at high cell densities, where function in slab gels quickly falls off. **c**, Primary rat hepatocytes (24×10^6 hepatocytes ml^{-1}) and stabilizing stromal fibroblasts in agarose gels (slab versus channeled) after eight days of culture were stained with a fluorescent live/dead assay (green, Calcein AM; red, Ethidium Homodimer). Cells survive at the gel perimeter and near perfused channels, and survival decayed deeper in the gels. Scale bar, 1 mm. **d**, Assessment of albumin secretion (top) and urea synthesis (bottom) by primary hepatocytes (16×10^6 ml^{-1}) in gels after eight days of culture demonstrated improved hepatic function in channeled gels compared with slab gels. Error bars represent standard error, *p*-values for channel versus slab gel comparisons: $* < 0.0051$; $‡ < 0.045$.

or therapeutic replacements of human tissues. However, with the exception of avascular or thin tissues, it has been difficult to achieve the cellular densities of native tissues (approximately 10–500 million cells ml^{-1}). The approach described here demonstrates an avenue for building and studying such tissue mimics, in which the vasculature seems not to constrain the design space for the tissue itself, allowing for arbitrary cell types, matrices, and their patterning. Coupled with advances in microfluidic device technologies[26,27], the controlled architecture of these engineered fluidic networks may also provide a means to directly examine the interplay between mass transport requirements of specific tissues and vascular architecture. Moreover, the facile and highly automated nature of this perfusable tissue fabrication strategy should provide a flexible platform for a wide array of specific applications, and may enable the scaling of densely populated tissue constructs to arbitrary size.

Methods

Preparation and 3D printing of carbohydrate glass. A mixture of 25 g glucose, 53 g sucrose, 10 g dextran (86 kDa), and 50 ml reverse osmosis water (≥18 MΩ; Millipore) was warmed to 165 °C to remove most of the water and form a liquid glass. The hot mixture was poured into a 50 ml syringe that was maintained at 110 °C. The syringe was mounted on a custom-modified RepRap Mendel 3D printer with associated electronics (Gen3, MakerBot; RAMPS + RAMMS, Ultimachine). Custom Python scripts were developed to generate the 3D motion control GCode used to drive the machine via open-source ReplicatorG software. Carbohydrate-glass lattices were printed at 110 °C under nitrogen pressure with pneumatic control through a 16-gauge or 18-gauge (1.2 mm or 0.84 mm ID, respectively) steel nozzle, vitrified to 50 °C, and then immersed in a 25 mg ml^{-1} solution of PDLGA (Purac) in chloroform for up to 5 min. Glass lattices were encapsulated in ECM along with living cells on the same day the lattices were fabricated, or were stored at 45 °C or in a vacuum chamber until use to protect the hygroscopic carbohydrates from absorbing ambient moisture under atmospheric conditions.

Polymer synthesis and cell and lattice encapsulation. Poly(ethylene glycol) diacrylate (PEGDA, 6 or 35 kDa) and acrylate-PEG-RGDS (4 kDa) were synthesized as previously described[18]. In a typical experiment, a prepolymer mixture containing PEGDA (5, 10 or 20 wt%), acrylate-PEG-RGDS (1 mM), photoinitiator (Irgacure 2959, Ciba Geigy, 0.05% w/v), and cells of interest ($1–40 \times 10^6$ cells ml^{-1}) was dispensed into rectangular moulds containing suspended carbohydrate-glass lattices (500 μl total volume per gel). PEG hydrogels were photopolymerized (Omnicure 2000, 320–500 nm) at 100 mW cm^{-2} for two repetitions of 30 s duration (rotating 180° about the *y* axis before the second exposure). Fibrin gels (10–40 mg ml^{-1}) were created by combining fibrinogen, thrombin and cell suspension in phosphate-buffered saline (PBS) and then dispensing this mixture around a carbohydrate-glass lattice. Fibrin gels were polymerized for 10 min at 37 °C or for 20 min at room temperature. Matrigel constructs were formed by mixing a cell suspension with Matrigel and then dispensing the mixture around a carbohydrate-glass lattice, followed by incubation at 37 °C for 10 min. Alginate gels (2%) were formed by mixing an alginate solution with cell suspension, dispensing the mixture around a carbohydrate-glass lattice, then carefully crosslinked with a 50 mg ml^{-1} $CaCl_2$ solution for 10 min. Agarose gels (2%) were formed by mixing a low-melt agarose solution with cell suspension, dispensing the mixture around a carbohydrate-glass lattice, then placed at 4 °C for 20 min. All crosslinked gels were post-processed identically: after crosslinking they were placed in complete medium to dissolve the carbohydrate glass (10 min), followed by exchange with fresh medium and cell culture (static culture or orbital shaking at a rate of 2 Hz). In 800 μm channels (diameter) we measured peak flow

rates of 10 μl s^{-1}, corresponding to mean velocities of 5 mm s^{-1} and shear stress of 1 dyn cm^{-2}. These values are comparable to physiologic settings. Gel slabs (without vascular architectures) were created by using identical rectangular moulds and identical gel processing steps, but without encapsulating glass lattices. Diffusion studies were conducted with fluorescent Cascade Blue Dextran 10 kDa (Invitrogen). Fluorescent beads (Polysciences) were mixed with ECM prepolymer mixtures for matrix immobilization or PBS for bead perfusion studies. Heparanized human blood, whole blood, or packed red blood cells (Interstate Blood Bank) were washed and diluted with PBS before use.

Endothelialization of vascular networks. HUVECs were seeded in the vascular lumen by injecting a HUVEC suspension (35×10^6 cells ml^{-1}) into the vascular architecture approximately 10 min after the constructs were fabricated. HUVECs were allowed to attach in static culture for one hour before introducing flow, and they reached confluence within one day. Endothelialized gels often contained additional HUVECs (1.5×10^6 ml^{-1}) and 10T1/2 cells (1.5×10^6 ml^{-1}) encapsulated in the bulk gel, such as the gel shown in Fig. 3c–f.

Received 25 October 2011; accepted 15 May 2012; published online 1 July 2012

References

1. Radisic, M. *et al.* Medium perfusion enables engineering of compact and contractile cardiac tissue. *Am. J. Physiol. Heart Circ. Physiol.* **286,** H507–H516 (2004).
2. Langer, R. & Vacanti, J. P. Tissue engineering. *Science* **260,** 920–926 (1993).
3. Griffith, L. G. & Swartz, M. A. Capturing complex 3D tissue physiology *in vitro*. *Nature Rev. Mol. Cell Biol.* **7,** 211–224 (2006).
4. Vunjak-Novakovic, G. & Scadden, D. T. Biomimetic platforms for human stem cell research. *Cell Stem Cell* **8,** 252–261 (2011).
5. Schmidt-Nielsen, K. Scaling in biology: The consequences of size. *J. Exp. Zool.* **194,** 287–307 (1975).
6. Golden, A. P. & Tien, J. Fabrication of microfluidic hydrogels using molded gelatin as a sacrificial element. *Lab Chip* **7,** 720–725 (2007).
7. Ling, Y. *et al.* A cell-laden microfluidic hydrogel. *Lab Chip* **7,** 756–762 (2007).
8. Choi, N. W. *et al.* Microfluidic scaffolds for tissue engineering. *Nature Mater.* **6,** 908–915 (2007).
9. Cuchiara, M. P., Allen, A. C. B., Chen, T. M., Miller, J. S. & West, J. L. Multilayer microfluidic PEGDA hydrogels. *Biomaterials* **31,** 5491–5497 (2010).
10. Visconti, R. P. *et al.* Towards organ printing: Engineering an intra-organ branched vascular tree. *Exp. Opin. Biol. Therapy* **10,** 409–420 (2010).
11. Therriault, D., White, S. R. & Lewis, J. A. Chaotic mixing in three-dimensional microvascular networks fabricated by direct-write assembly. *Nature Mater.* **2,** 265–271 (2003).
12. Bellan, L. M. *et al.* Fabrication of an artificial 3-dimensional vascular network using sacrificial sugar structures. *Soft Matter* **5,** 1354–1357 (2009).
13. Wu, W. *et al.* Direct-write assembly of biomimetic microvascular networks for efficient fluid transport. *Soft Matter* **6,** 739–742 (2010).
14. Reinheimer, M. A., Mussati, S. & Scenna, N. J. Influence of product composition and operating conditions on the unsteady behavior of hard candy cooling process. *J. Food Eng.* **101,** 409–416 (2010).
15. Lutolf, M. P. & Hubbell, J. A. Synthetic biomaterials as instructive extracellular microenvironments for morphogenesis in tissue engineering. *Nature Biotechnol.* **23,** 47–55 (2005).
16. Tibbitt, M. W. & Anseth, K. S. Hydrogels as extracellular matrix mimics for 3D cell culture. *Biotechnol. Bioeng.* **103,** 655–663 (2009).
17. Heiber, J., Clemens, F., Graule, T. & Hülsenberg, D. Thermoplastic extrusion to highly-loaded thin green fibres containing $Pb(Zr,Ti)O_3$. *Adv. Eng. Mater.* **7,** 404–408 (2005).
18. Miller, J. S. *et al.* Bioactive hydrogels made from step-growth derived PEG-peptide macromers. *Biomaterials* **31,** 3736–3743 (2010).
19. Moon, J. J., Hahn, M. S., Kim, I., Nsiah, B. A. & West, J. L. Micropatterning of poly(ethylene glycol) diacrylate hydrogels with biomolecules to regulate and guide endothelial morphogenesis. *Tissue Eng. Part A* **15,** 579–585 (2009).
20. DeLong, S. A., Moon, J. J. & West, J. L. Covalently immobilized gradients of bFGF on hydrogel scaffolds for directed cell migration. *Biomaterials* **26,** 3227–3234 (2005).
21. Stefonek, T. J. & Masters, K. S. Immobilized gradients of epidermal growth factor promote accelerated and directed keratinocyte migration. *Wound Repair Regen.* **15,** 847–855 (2007).
22. Leslie-Barbick, J. E., Moon, J. J. & West, J. L. Covalently-immobilized vascular endothelial growth factor promotes endothelial cell tubulogenesis in poly(ethylene glycol) diacrylate hydrogels. *J. Biomater. Sci. Poly. Edn* **20,** 1763–1779 (2009).
23. Sundararaghavan, H. G., Monteiro, G. A., Firestein, B. L. & Shreiber, D. I. Neurite growth in 3D collagen gels with gradients of mechanical properties. *Biotechnol. Bioeng.* **102,** 632–643 (2009).
24. Nemir, S., Hayenga, H. N. & West, J. L. PEGDA hydrogels with patterned elasticity: Novel tools for the study of cell response to substrate rigidity. *Biotechnol. Bioeng.* **105,** 636–644 (2010).
25. Tsang, V. L. *et al.* Fabrication of 3D hepatic tissues by additive photopatterning of cellular hydrogels. *FASEB J.* **21,** 790–801 (2007).
26. Thorsen, T., Maerkl, S. J. & Quake, S. R. Microfluidic large-scale integration. *Science* **298,** 580–584 (2002).
27. Atencia, J. & Beebe, D. J. Controlled microfluidic interfaces. *Nature* **437,** 648–655 (2005).

Acknowledgements

We thank the large number of open source and related projects that critically facilitated this work, including Arduino.cc, RepRap.org, MakerBot.com, Replicat.org, MakerGear.com, Ultimachine.com, Hive76.org, Python.org, Hugin.SourceForge.net, ImageMagick.org, Blender.org, Enblend.sourceforge.net, NIH ImageJ, and Fiji.sc. We thank R. J. Vlacich and C. D. Thompson for assistance with precision pneumatic extrusion, A. Dominguez for assistance with red blood cell isolation, and Y-J. Chen for assistance with transduction. This work was supported in part by grants from the US National Institutes of Health (EB00262, EB08396, GM74048), the Penn Center for Engineering Cells and Regeneration, and the American Heart Association-Jon Holden DeHaan Foundation. Individual fellowship support was provided by R. L. Kirschstein National Research Service Awards from NIH (J.S.M., HL099031; K.R.S., DK091007), the National Science Foundation IGERT program (M.T.Y., DGE-0221664), and the American Heart Association (X.Y., 10POST4220014).

Author contributions

J.S.M. and C.S.C. conceived and initiated the project. J.S.M., K.R.S., M.T.Y., B.M.B., D-H.T.N., D.M.C., E.T., A.A.C., P.A.G., X.Y., and R.C. designed and performed experiments. C.S.C. and S.N.B. supervised the project.

Additional information

The authors declare no competing financial interests. Supplementary information accompanies this paper on www.nature.com/naturematerials. Reprints and permissions information is available online at www.nature.com/reprints. Correspondence and requests for materials should be addressed to C.S.C.

nature materials

SUPPLEMENTARY INFORMATION

DOI: 10.1038/NMAT3357

Rapid casting of patterned vascular networks for perfusable engineered three-dimensional tissues

Supplementary Methods and Figures

S1. Encapsulation of gradients of cells and immobilized factors

Opposing gradients of cells and immobilized factors (**Supplementary Figure 1**) were fabricated by first positioning a carbohydrate glass lattice in a vertical orientation between two glass slides. Five aliquots of different concentrations of cells and fluorescent beads were created in eppendorf tubes containing a constant concentration of low-melt agarose (see main text) maintained at 37 °C. Cell concentrations ranged from 3e6 cells/mL to 3e5 cells/mL across the aliquots. The aliquots were then serially dispensed into the mold containing the carbohydrate glass lattice which was maintained at room temperature. Delay time between dispensing operations allowed the matrix to partially solidify before the next dispensing operation. After complete gelation (incubation at 4 °C, see main text) the gel was removed from the chamber and processed as described in the main text for uniform gels.

S2. Lentiviral reporters

Lentiviral reporter constructs were generated using Multi-site Gateway recombination (Invitrogen) into a Gateway-compatible version of the third generation lentiviral vector, pRRL [1], in which the CMV sequence was replaced with the R4R2ccdB cassette from pLENTI6 (Invitrogen). Entry clones were generated using the following entry vectors, pENTR5 and pENTR-DTOPO (Invitrogen). cDNAs were constructed from CMV promoter (pCDNA3.1, Invitrogen), destabilized EGFP (pCAG-GFPd2) [2, 3], Gaussia luciferase (pGluc-Basic, NanoLight Technology), EGFP, and IFP-IRES-mCherry (generous gift of Roger Tsien) [4]. pRRL-based reporter lentiviruses were produced in 293T cells co-transfected with the second-generation packaging vectors psPAX2 and pMD2.G (Addgene).

S3. Hepatocyte isolation and maintenance

Rat hepatocytes were isolated from 2-3 month old adult female Lewis rats (Charles River) by collagenase perfusion using methods described previously [6, 7]. Briefly, animals were anesthetized with isoflorane and the portal vein was cannulated. The liver was perfused and digested

DOI: 10.1038/NMAT3357

with collagenase. Hepatocytes were purified from the digest using Percoll centrifugation and then seeded at a density of 0.5e6 per well of a six well plate adsorbed with 0.14 mg/ml rat tail Collagen-1 (BD Biosciences). The following day, J2-3T3 fibroblasts were added to hepatocyte cultures (ratio of 1:1). Co-cultures were maintained in 'hepatocyte medium' (see below) for 7-10 days prior to encapsulation in perfusable or non-perfusable agarose gels as described in the main text.

S4. Hepatocyte function

Rat albumin in sampled media was quantified by enzyme-linked immunosorbant assay (ELISA) using a rat albumin ELISA kit (Bethyl labs). Urea in sampled media was measured by acid- and heat-catalyzed condensation of urea with diacetylmonoxime to give a colored-product that was measured spectophotometrically (Urea Nitrogen kit; StanBio Labs). For imaging, hepatic hydrogels were sliced into approximately 1 mm slices and then incubated with calcein-AM ("live", 5 μg/ml, Invitrogen) and ethidium homodimer ("dead", 2.5 μg/ml, Invitrogen) for 30 minutes and washed before imaging.

S5. Imaging and Image montage generation

Engineered scaffolds were imaged on an epifluorescence microscope (TE-200, Nikon) or a confocal microscope (LSM 710, Zeiss). Epifluorescence image montages were generated using a combination of automated and manual control point generation and adjustment with autopano-sift-c (2.5.0) and the open-source Hugin software (2010.2.0) to remove spherical aberration and vignetting from each image before adjacent image fusion. Overlays and composite images were created with the open source ImageMagick software. Confocal image montages were automatically generated by microscope control software during image acquisition (ZEN, Zeiss). Fluorescence normalization aided in visualization and discrimination of cell type throughout deep confocal image stacks (**Figure 3c,e,f**) and was accomplished by the open source Enfuse software.

S6. Cell maintenance

Human umbilical vein endothelial cells (HUVECs, Lonza; Basel, Switzerland) and C3H/10T 1/2 cells were maintained in complete Endothelial Growth Medium-2 (EGM-2; Lonza). Human Embryonic Kidney (HEK 293T) cells were maintained in Dulbecco's modified Eagle medium containing 10% fetal bovine serum (FBS), 2 mM L-glutamine, 1000 U/mL penicillin, and 100 mg/L streptomycin at 37 °C/5% CO_2. Hepatocytes were maintained in 'hepatocyte medium' containing DMEM with high glucose (4.5 g/L), 10% (v/v) bovine serum (Gibco), 0.5 U/ml

insulin (Lilly), 7 ng/ml glucagons (Bedford Laboratories), 7.5 μg/ml hydrocortisone (Sigma), and 1% penicillin-streptomycin.

DOI: 10.1038/NMAT3357

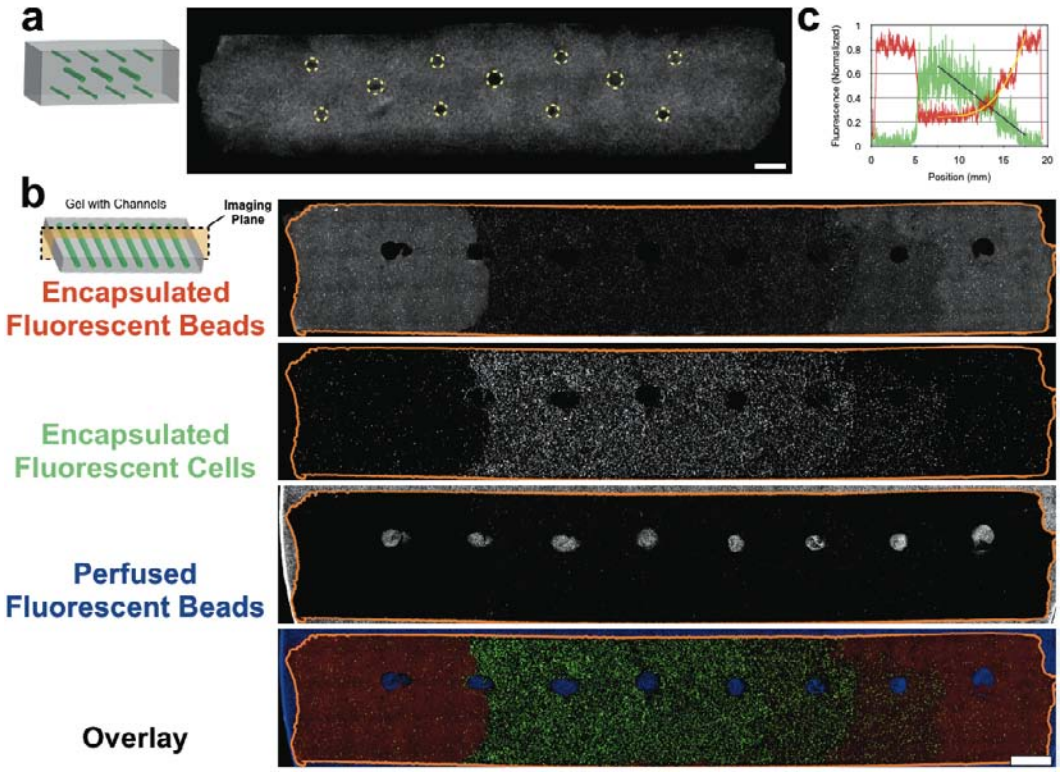

Supplementary Figure 1: Multilayer vascular channels and complex cellular and immobilized factor gradients in engineered tissues. **(a)** 3D multilayer architectures were fabricated in cellularized gels. Here, 10T1/2 cells expressing EGFP were encapsulated in fibrin (40 mg/mL) at 2.5e6 cells/mL and then cross-sectioned for epifluorescent cell imaging and image-montage generation. Perfusable channels are highlighted (dotted yellow lines). Scale bars = 1 mm. **(b)** Complex gradients of immobilized factors (fluorescent beads, red) and cells (expressing EGFP, green) can be fabricated in a single scaffold independently from the channel architecture (fluorescent beads, blue). The gel boundary is outlined in orange and images represent a maximum intensity projection of a 256 μm z-stack automated montage. Scale bar = 1 mm. **(c)** Line plots of normalized fluorescence across the construct from **(b)** indicates that step, linear, and exponential gradients of cells (green) and immobilized factors (red) were readily generated in a single perfusable engineered tissue construct. Trendlines for the linear and exponential regimes (purple line, cells; yellow line, beads) showed good correlation with these gradients (R^2 for linear cell gradient = 0.75; R^2 for exponential bead gradient = 0.93). Here, cells were encapsulated along with immobilized fluorescent beads as a model factor but this technology should be readily translated to immobilized gradients of adhesive peptides, proteins and growth factors, or the ECM itself. Scale bar = 1 mm.

COMSOL Model of Nutrient Uptake in Vascular Hydrogels (model nutrient = O_2)

Assumptions

- Steady-state
- No υ change in Θ
- Fully developed flow
- Symmetry everywhere
- Flux and concentration matching
- D constant
- Uptake is governed by Michaelis-Menten kinetics
- Use oxygen as model nutrient

Governing Equation

$$\frac{\partial C_i}{\partial t} = D\nabla^2 C_i - \underline{\upsilon}\cdot\nabla C_i + R$$

in Hydrogel

$$\frac{\partial C_{HYD}}{\partial t} = D_{eff}\nabla^2 C_{HYD} + R$$

$$0 = D_{eff}\left[\frac{1}{r}\frac{\partial}{\partial r}\left(r\frac{\partial C_{HYD}}{\partial r}\right) + \frac{\partial^2 C_{HYD}}{\partial z^2}\right] - \frac{v_{\max} C_{HYD}}{K_M + C_{HYD}}$$

Low Uptake Rate (Low Cell Concentration)

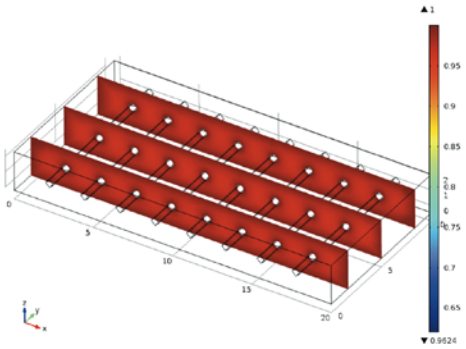

High Uptake Rate (High Cell Concentration)

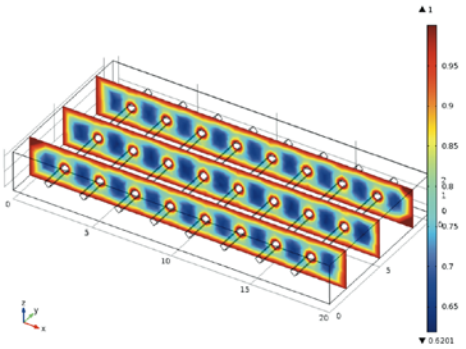

Supplementary Figure 2: Finite element model of nutrient consumption by encapsulated cells in the interstitial space of perfusable hydrogels (using oxygen as a model nutrient). The model was implemented in COMSOL by starting with the governing mass transport equation, inputting the listed assumptions to simplify, and applying to the given hydrogel geometry with accompanying boundary conditions to solve. Exploration of the model in COMSOL indicates that at low nutrient uptake rate (corresponding to low cell concentrations), the nutrient concentration is high everywhere in the gel, while at high nutrient uptake rate (corresponding to high cell concentrations), nutrient concentration is high at the gel perimeter and radially around perfused channels. The nutrient concentration profile observed in this model is consistent with the empirical data presented in **Figure 4**.

DOI: 10.1038/NMAT3357

References

[1] Barry, S. C., Harder, B., Brzezinski, M., Flint, L. Y., Seppen, J. & Osborne, W. R. Lentivirus vectors encoding both central polypurine tract and posttranscriptional regulatory element provide enhanced transduction and transgene expression. *Hum Gene Ther* **12**, 1103–8 (2001).

[2] Li, X., Zhao, X., Fang, Y., Jiang, X., Duong, T., Fan, C., Huang, C. C. & Kain, S. R. Generation of destabilized green fluorescent protein as a transcription reporter. *J Biol Chem* **273**, 34970–5 (1998).

[3] Matsuda, T. & Cepko, C. L. Controlled expression of transgenes introduced by in vivo electroporation. *Proc Natl Acad Sci USA* **104**, 1027–32 (2007).

[4] Shu, X., Royant, A., Lin, M. Z., Aguilera, T. A., Lev-Ram, V., Steinbach, P. A. & Tsien, R. Y. Mammalian expression of infrared fluorescent proteins engineered from a bacterial phytochrome. *Science* **324**, 804–7 (2009).

[5] Miller, J. S., Shen, C. J., Legant, W. R., Baranski, J. D., Blakely, B. L. & Chen, C. S. Bioactive hydrogels made from step-growth derived peg-peptide macromers. *Biomaterials* **31**, 3736–43 (2010).

[6] March, S., Hui, E. E., Underhill, G. H., Khetani, S. & Bhatia, S. N. Microenvironmental regulation of the sinusoidal endothelial cell phenotype in vitro. *Hepatology (Baltimore, Md)* **50**, 920–928 (2009).

[7] Chen, A. A., Thomas, D. K., Ong, L. L., Schwartz, R. E., Golub, T. R. & Bhatia, S. N. Humanized mice with ectopic artificial liver tissues. *Proceedings of the National Academy of Sciences of the United States of America* **108**, 11842–11847 (2011).